AstroComb(v.1.0): Non-linear, Multi-channel, Probabilistic Cyclostratigraphic Analysis

Iris Fernandes*[1], Klaus Mosegaard*[1], Aske L. Sørensen[2], Mohammad Youssof[1], Nicolas Thibault[2], and Tais W. Dahl[2]

[1]Niels Bohr Institute, University of Copenhagen, Denmark
[2]Department of Geosciences and Natural Resource Management, University of Copenhagen, Denmark

Abstract

We present a new algorithm for constructing floating astronomical timescales with explicit uncertainty estimates from sedimentary sequences. The method integrates probabilistic spectral analysis with inverse geochronological modelling, applied to ultra-high-resolution, multi-proxy datasets such as core scanning X-Ray Fluorescence (XRF) elemental records. Our framework does not smooth data or impose layer-to-layer dependency, allowing sedimentation rates to vary abruptly at short stratigraphic length scales. By detecting and statistically constraining Milankovitch cycles preserved in stratigraphic signals, the algorithm seeks a floating age-depth model that reconstructs geological time and can be anchored to deliver absolute age assignment, when astronomical tie points and/or radiometric ages are available. The resulting timescales enable precise, uncertainty-bounded timing of biostratigraphic zones, geochemical events, and depositional cycles. This approach advances astrochronology by combining cycle detection with formal stratigraphic modelling, while preserving fine-scale depositional variability, offering a reproducible and statistically rigorous framework for dating deep-time records.

1 Introduction

Astronomical forcing of Earth's climate system produces quasi-periodic variations in sedimentary records that can be used to construct geological timescales, reconstruct daylength, Earth system evolution, and investigate the long-term dynamics of the Solar System (Hinnov et al., 2013 and references therein). Astrochronology has therefore become a central component of modern geochronology and is now widely used in calibration of the Geological Timescale (Laskar, 2020), reconstruction of past climate variability (Hays et al., 1976; Pälike

*Corresponding authors: iris@nbi.ku.dk, mosegaard@nbi.ku.dk

et al., 2006), and studies of Earth–Moon distance and Solar System evolution (Ma et al., 2017; Meyers and Malinverno, 2018; Zhou et al., 2024). Improvements in astrochronological methodologies therefore have implications extending beyond stratigraphy, influencing multiple areas of geoscience and planetary science.

The fundamental challenge in astrochronology is that sedimentary records preserve orbital forcing only indirectly. Variability in sedimentation rates, changes in depositional environments, diagenetic overprinting, and nonlinear sedimentary responses distort the astronomical signals. Furthermore, in deep-time studies beyond approximately 50–60 Ma, where theoretical orbital solutions become unreliable due to the chaotic evolution of the Solar System (Laskar et al., 2004, 2011). As a result, astrochronology requires inverse methods that infer sedimentation histories and test consistency with orbital forcing.

Over the past two decades, several classes of inverse astrochronologic methods have been developed to address this problem. Early methods, such as Average Spectral Misfit (ASM) evaluates spectral peaks against astronomical frequencies across sedimentation rates and was later extended to moving-window analysis (eASM; Meyers and Sageman 2007).

Bayesian spectral methods later formalized this framework by evaluating the power concentrated in astronomical frequencies relative to a noise model formulated as a likelihood function (Malinverno et al., 2010; Peng et al., 2023; Trayler et al., 2024). Parallel developments introduced time-domain approaches including `TimeOpt` (Meyers, 2015) and time-variant sinusoidal modeling (Sinnesael et al., 2016; `ACE v.1`) along with extensions (Sinnesael et al., 2018; Meyers and Malinverno, 2018; Malinverno and Meyers, 2024; Hoang et al., 2025), while correlation-based methods such as `COCO` and `eCOCO` evaluated agreement between measured and theoretical power spectra (Li et al., 2018). More recently, AstroGeoFit has introduced a unified, uncertainty-aware framework that jointly optimizes sedimentation rates and astronomical tuning, enabling rigorous error estimation in age–depth models (Hoang et al., 2025). Together these methods have substantially advanced quantitative astrochronology and uncertainty assessment.

Sedimentation is an inherently unsteady and discrete process, influenced by short-lived hiatuses and implicit erosion that result in nonlinear time-depth relationships across all time scales (Kemp and Sexton, 2014). Mass accumulation is affected by deposited grains and diagenetic processes inside the sediments, including cementation, authigenic mineral formation and recrystallization. Milankovitch insolation forcing may influence deposited grains as well as diagenetic products. The sediment composition is also affected by other cyclic processes, for example biogeochemical resonances and local autogenic deposition processes (Zhao et al., 2023; Paola, 2016; Munnecke et al., 2001). These processes may introduce abrupt local variations in mass accumulation rates that are difficult to capture using approaches that assume smoothly varying sedimentation. In the following, we use "sedimentation rates" to refer broadly to all mass-accumulation rates in a sedimentary drill core.

We introduce `AstroComb` —a probabilistic framework for combing multi-channel geochemical records to identify signatures of astronomical periodicities. The goal is to construct floating astronomical timescales and to estimate sedimentation rates within stratigraphic sections while explicitly quantifying the associated uncertainties. Conceptually, AstroComb builds on the Bayesian spectral inversion approach of (Malinverno et al., 2010) but extends it in several important ways.

First, the method simultaneously incorporates multiple observational channels, allowing

information from independent geochemical proxies to constrain sedimentation-rate estimates. Second, the method allows abrupt local variations in sedimentation rate where supported by the data. Third, the framework explicitly quantifies uncertainty by estimating full posterior probability distributions for sedimentation rates at every stratigraphic position. The current version of `AstroComb` looks for multiple periodic signals with the correct relative periods for selected astronomical insolation forcings, and is currently not designed to independently validate whether such fit is indeed driven by insolation variations, e.g. by seeing eccentricity-driven amplitude modulations on precession and/or obliquity cycles.

The `AstroComb` method operates through a sliding-window probabilistic inversion in which observed local spectra are compared with target astronomical frequencies under a range of candidate sedimentation rates. The resulting posterior distributions provide estimates of sedimentation rates, uncertainty, and information content as a function of stratigraphic depth.

We evaluate the performance of `AstroComb` first by using synthetic datasets designed to test the recovery of abrupt sedimentation-rate changes under substantial noise contamination. Then, we apply `AstroComb` to ultra-high-resolution X-ray fluorescence (XRF) data from the upper Cambrian Alum Shale Formation of Scandinavia. The Alum Shale represents an ideal test case because of its preservation of orbital-scale cyclicity (Sørensen et al., 2020; Zhao et al., 2022). Using approximately 90,000 measurements spanning ∼19 m of stratigraphy, we evaluate whether probabilistic multi-channel analysis can recover orbitally forced signals while recovering variability in sedimentation rates.

2 Theory and Methods

2.1 Overview

The goal of this study is to reconstruct a *locally varying sedimentation rate profile with errorbars* from multiple geochemical depth series, under the assumption that certain stratigraphic signals (e.g., elemental variability) reflect astronomical forcing. We achieve this by inverting a forward model of signal distortion under varying sedimentation, using a formulation rooted in probabilistic inversion.

This method builds upon the principles of astrochronology, particularly the spectral identification of Milankovitch-band periodicities in sedimentary records, but extends them to allow for *instantaneous, non-stationary* sedimentation rates. `AstroComb` performs a sliding-window probabilistic fit of observed geochemical spectra to a predefined target astronomical spectrum, yielding a sedimentation rate for the mid-point in the window that optimally "stretches" or "compresses" the time axis at each position to recover astronomical frequencies. The fit is performed in frequency domain, which allows multi-channel (e.g. multiple elements) that will not be obscured if displaced by a phase-lag.

We begin by formalizing the relationship between sedimentation rate and spectral distortion, then describe the inversion procedure and implementation of `AstroComb`. Finally, as an example, we discuss its application to the Alum Shale data and compare to previous cyclostratigraphic results (Sørensen et al., 2020).

2.2 Forward Model of Spectral Distortion

Let $d(z)$ be a geochemical depth series (e.g., Al concentrations), where z is stratigraphic depth. If sediment accumulated at a locally constant rate, $r(z) = \frac{dz}{dt}$, then in the time domain, the corresponding series is $d(t)$. However, in practice we only observe the signal in the depth domain.

Let k be a frequency in the depth domain (wave number in cycles per mm) and f its time-domain counterpart (cycles per ky). The transformation between the two is:

$$k = \frac{f}{r} \tag{1}$$

Thus, a fixed astronomical frequency f will appear in the stratigraphic record as a peak at k, depending on the local sedimentation rate. Variations in $r(z)$ distort the signal, shifting, splitting, or smearing spectral peaks (Schiffelbein and Dorman, 1986; Ripepe and Fischer, 1991; Herbert, 1994; Meyers et al., 2001). Our objective is to recover $r(z)$ such that the observed power spectrum matches that predicted from astronomical forcing (see Figure 1).

2.3 Computing the Likelihood of a Sedimentation Rate

For a given depth interval (window) centered at z_0, we obtain power spectra $\mathbf{D}_{obs}$ of multiple, observed signals ($\mathbf{D}_{obs}$ is a matrix of spectra with a spectrum of one channel in each column). For each trial sedimentation rate r, we convert the target time-domain frequencies f to expected depth-domain frequencies (wave numbers) $k = f/r$ and compute *synthetic spectra*

$$\mathbf{G}(r, \mathbf{a}) = \sum_{m=1}^{M} \mathrm{a}_m \mathbf{w}\left(\frac{f_m}{r}\right) \tag{2}$$

where $\mathbf{G}(r, \mathbf{a})$ is a matrix of synthetic data spectra (a copy of the spectrum in each column), f_m is the m'th Milankovitch frequency (assumed known), and $\mathbf{w}(\frac{f_m}{r})$ and $\mathbf{a}$ are vectors with the shape of the spectral lines, centered at $\frac{f_m}{r}$, and the corresponding amplitudes, respectively. The shape $\mathbf{w}$ can be computed as the discrete Fourier transform of a discretized delta function with the same length as the window.

From the synthetic spectra $\mathbf{G}(r, \mathbf{a})$ and the matrix of observation spectra $\mathbf{D}_{obs}$ we can now calculate the likelihood as the probability of data, given the sedimentation rate r and the spectral peak amplitudes $\mathbf{a}$:

$$L(r, \mathbf{a}) = P\left(\mathbf{D}_{obs} | (r, \mathbf{a})\right). \tag{3}$$

In our computation of the likelihood, data uncertainties are provided by the user as the probability that a peak in the observed spectrum is a Milankovitch peak. Existing data-fitting-based methods (Meyers and Sageman 2007, Malinverno et al. 2010; `TimeOpt`: Meyers 2015; `TimeOptMCMC`: Meyers and Malinverno 2018; `AstroGeoFit`: Hoang et al. 2025) are purely based on misfits between data (elemental records) and synthetic signals (generated from assumed Milankovitch periods), but AstroComb is instead aimed at simulating the data uncertainty evaluation carried out by practitioners analyzing observational data. In traditional misfit calculations you not only need experimental uncertainties, but also components

of the data that are not modeled by the Milankovitch cycles. The latter are significant, but not directly available (for example, The `TimeOptMCMC` algorithm estimates them through a Hierarchical Bayes approach (Meyers and Malinverno, 2018). However, in our approach we are automatically taking all data uncertainty sources into account, including the practitioner's confidence in identifying spectral peaks.

The most (almost universally adopted) definition of the likelihood is

$$L(\mathbf{m}) = p_n(\mathbf{d}_{obs} - g(\mathbf{m})) \ , \tag{4}$$

where p_n is the noise distribution, $\mathbf{d}_{obs}$ is the observed data, and $g(\mathbf{m})$ is the forward function mapping the unknown model parameters $\mathbf{m}$ into the data. We can see from equation 4 that the likelihood depends on $\mathbf{m}$ through the function g, so we can define a function p_d such that

$$p_d(g(\mathbf{m})) \equiv L(\mathbf{m}). \tag{5}$$

Since $g(\mathbf{m})$ is the "noise-free data", we can view p_d as the (possibly unnormalized) distribution of the noise-free data, given that we only know the observations $\mathbf{d}_{obs}$ and the data uncertainties p_n. However, definition 5 also shows that a likelihood can be calculated by any procedure that measures the goodness of fit, based on a forward function g and observations $\mathbf{d}_{obs}$. The underlying uncertainty need not be given in advance through a noise distribution p_n. If the goodness of fit is *a priori* acceptable for the analyst (e.g., based on experience), p_n can be determined afterwards, if needed. In the following we follow a procedure where we define the likelihood without an initial definition of p_n.

Our likelihood calculation is as follows:

1. As prior information about the data uncertainties, we mimic the 'manual' process of spectral line identification by defining a probability that there is a potential Milankovitch peak at a given wavenumber k in the spectrum. Between user-defined lower and upper bounds a (the lower limit for being identified as a "peak") and b (the value above which we are sure that we have found a potential peak), the probability increases from a user defined, small positive number p_a at the lower limit to $p_b = 1 - p_a$ at the upper limit. Typical values are $a = \langle F \rangle + \sigma_F$ and $b = \langle F \rangle + 3\sigma_F$, where $\langle F \rangle$ is a local mean of the spectrum around the considered wavenumber k over an interval of length 1, and σ_F is the local standard deviation of the spectrum. A typical value of the threshold probability p_a is 0.01. The probability is chosen as a smooth, monotonically increasing sigmoid function $p(x)$ satisfying

$$p(a) = p_a, \qquad p_b(b) = 1 - p_a, \tag{6}$$

with the constraints

$$b > a, \qquad 0 < p_a < 0.5. \tag{7}$$

We adopt the logistic sigmoid form

$$p(x) = \frac{1}{1 + \exp\big(-k(x - x_0)\big)} \tag{8}$$

with

$$x_0 = \frac{a + b}{2}. \tag{9}$$

2. For each layer (which is $\Delta z = 0.2$ mm thickness in the Fågeltofta-2 core), we evaluate the likelihood in a grid of sedimentation rates r with typical grid spacing $\Delta r = 0.02$ mm/ky. Each possible choice corresponds to given locations of the Milankovitch cycles in the spectrum, and for each location at k_i with spectral amplitude a_i, we evaluate the probability $p(k_i, a_i)$. Finally, the likelihood of the considered sedimentation rate $\mathbf{r}$ is computed as the product

$$L(\mathbf{r}) = \prod_{i=1}^{I_M} p(k_i, a_i), \tag{10}$$

where I_M is the number of Milankovitch cycles considered. For example, when several records of major element concentrations are used in the calculation, the combined likelihood for all records is computed as the product of the individual likelihoods. That is, we can assume channels are independent of each other.

2.4 The Posterior Probabilities of Sedimentation Rates

If prior information about $(r, \mathbf{a})$ is encoded by a probability density $\rho(r, \mathbf{a})$ we can - in a Bayesian formulation - express the complete, probabilistic solution as a *posterior* probability density

$$p(r, \mathbf{a}) = C \cdot L(r, \mathbf{a})\, \rho(r, \mathbf{a}). \tag{11}$$

where C is a proportionality constant. In the example below, where data from Fågeltofta-2 is analyzed, the prior assigns constant values to all sedimentation rates within user-defined boundaries of 1.0 mm/ky $< r <$ 10.0 mm/ky.

From the marginal sedimentation rate distribution

$$p(r) = \int p(r, \mathbf{a})\ da \tag{12}$$

at each stratigraphic position, we can now compute a floating geological time, t, and its uncertainties as a function of depth, z. If the absolute time, t_0, is known at a given depth z_0, and the sedimentation rate in layer n is r_n, the time at $z_0 + N\Delta z$ is

$$t(z_0 + N\Delta z) = t_0 + \Delta z \sum_{n=1}^{N} \frac{1}{r_n}\ . \tag{13}$$

From the posterior probability densities of the sedimentation rates r_n, and hence $\Delta z / r_n$, we can now calculate the uncertainties of the times, t. From the variances of the distributions of $\Delta z / r_n$ for all layers n, we can obtain the variance of $t(z_0 + N\Delta z)$ by a simple summation:

$$Var(t(z_0 + N\Delta z)) = \sum_{n=1}^{N} Var\left(\frac{\Delta z}{r_n}\right)\ . \tag{14}$$

Working with variances, instead of the full probability distributions for the inverse sedimentation rates, saves computer storage and time when processing large data sets. Furthermore, due to the central limit theorem, the distribution of the sum of random time increments

will converge to a Gaussian distribution when the number of layers increases, making the variance an adequate description of the uncertainty.

Finally, we calculate the Kullback-Leibler information measure at each depth z showing how much Milankovitch information is present in the data as a function of depth (Kullback and Leibler, 1951). This is obtained from:

$$\mathcal{I} = \int_R p_z(r) \ln \left(\frac{p_z(r)}{u(r)} \right) dr \tag{15}$$

where $p_z(r)$ is the calculated probability distribution of r at depth z, R is the range of sedimentation rates, and $u(r)$ is a uniform (constant, and hence non-informative) distribution. Theoretically, the Kullback-Leibler information measures the expected number of yes/no questions needed to update our state of information from what is given by $u(r)$ (here total ignorance) to what is given by $p_z(r)$ (here, the posterior distribution).

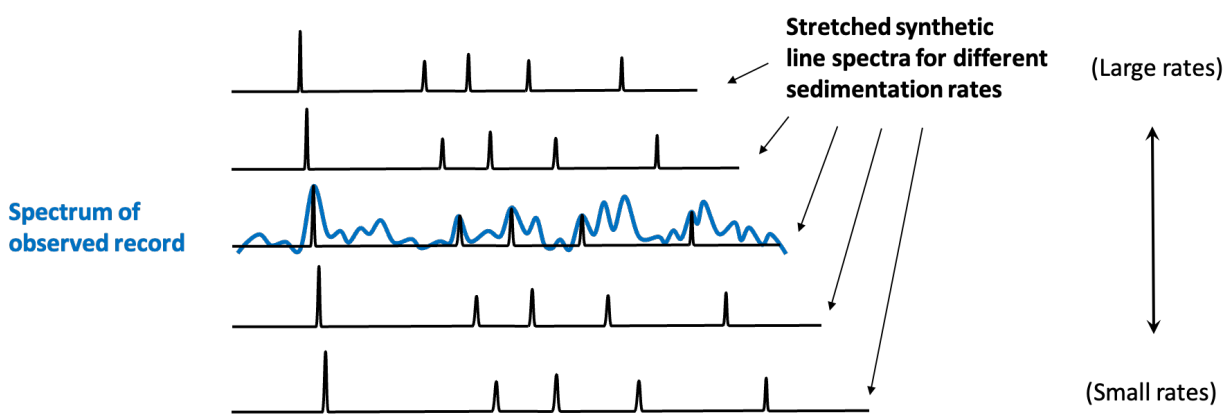

Figure 1: Schematic overview of the likelihood calculation for fitting Milankovitch cycles in elemental profiles. The spectrum of the observed geochemical signal (e.g., Al content) is compared against a theoretical line spectrum, composed of known astronomical frequencies, and stretched according to the sedimentation rate. The likelihood of each assumed sedimentation rate is computed from the probabilities that amplitudes at line locations are significant peaks. This process yields probability distributions of sedimentation rates as a function of depth, and allows an age–depth model consistent with Milankovitch forcing to be computed.

2.5 The AstroComb Algorithm

AstroComb implements the above approach through the following steps:

1. **Preprocessing**: Detrend and normalise the depth series, optionally re-sample or smooth.

2. **Sliding Window**: For each depth window (an interval with length, e.g., 2–4 m chosen by the user), compute the local power spectrum.

3. **Spectral Inversion**: Fit the observed spectrum to the target astronomical model. (The user defines the number of relevant Milankovitch periods). Based on spectral peak identification (the threshold of which is defined by the user), estimate the posterior probability distribution of the sedimentation rate.

4. **Output**: Store the sedimentation rate $r(z)$ and its posterior probability distribution for the window.

   Steps 1-4 in our calculation is accompanied by an uncertainty estimate. For each position of the sliding data window, the algorithm automatically estimates the part of the signal that cannot be attributed to Milankovitch forcing (see the likelihood calculation above).

5. **Construction of (floating) age-model**: Calculate geological time from sedimentation rates and stratigraphic thickness. Also, an age-depth model is derived when the user defines an age-depth anchor.

2.6 Target Astronomical Spectrum

Because no closed form astronomical solution exists beyond about 50 Ma (Laskar et al., 2011, 2004), we ignore the relative phases and adopt theoretical periods constructed from studies of deep-time orbital mechanics (Farhat et al., 2022; Waltham, 2015). For the upper Cambrian $\sim$ 497 Ma, the target includes:

- Long eccentricity: 405 ky
- Short eccentricity: 99 ky
- Obliquity: 32.4 ky
- Precession: 19.5 ky

We encode these as 4 sinusoids with known periods (without uncertainties). We do not define their expected spectral power ratios based on orbital modulation transfer, since the Earth's climate and environmental response to the Milankovitch forcing modifies these ratios in an unknown way.

3 Results

3.1 Synthetic data: dealing with discontinuous sedimentation rates

A test on synthetic data was carried out to study the accuracy and stability of the algorithm. More importantly, this allows us to validate whether we can reproduce a known sedimentation rate profile using a known target astronomical spectrum.

A severe test with artificial data forced by a sinusoidal Cambrian Milankovitch forcing overlain by 200% red noise and showing significant sedimentation rate discontinuities, was carried out (figure 2). The synthetic data were calculated from eq. 2 using approximate

Cambrian Milankovic frequencies $f_m = 1/T_m$ where $T_m = 405, 95, 124, 41, 25.7, 112, 100$ (all in ky), and with all amplitudes a_m set to 1. The synthetic sedimentation rate model (figure 3) is characterized by layers with sedimentation rates separated by significant discontinuities which could reflect abrupt changes in the climate such as going from coarse grained quartz sand to fine-grained mudrock and/or a pause in sedimentation (hiatus) that may also leave a geochemical imprint on the XRF data. From this model, the synthetic data were calculated (figure 3). The 200% noise was red noise with a $1/f^2$ power spectral density, simulating a background spectrum of geological signal that cannot be explained as astronomical forcing. Figure 3 shows the posterior probability densities of sedimentation rates for all depths, computed by `AstroComb` using the synthetic data. The true result (the synthetic reference model) is overlain to show the fidelity of the reconstruction.

Considering the relatively high noise level, the reconstruction of the true sedimentation rates is excellent. Abrupt changes in the sedimentation rate of about a factor three occur at 70, 74, 81, and 83 m, all of which are accurately captured by the `AstroComb` algorithm (figure 3). Sedimentation rates are not "smoothened", but the timing of the abrupt change appears uncertain.

However, the test also illustrates how the probability distribution outside the correct sedimentation rate is not invariable or zero. In fact, artifacts (mathematically possible, but incorrect sedimentation rates) are introduced by the noise, the variability of the true model, window size, and the non-linearity of the problem. Some of these artifacts show up as spurious parallel features that could potentially be misinterpreted as representing true sedimentation rates. This highlights a key challenge in cyclostratigraphic analyses: a given cycle may be interpreted as corresponding to different target periods, resulting in a multimodal sedimentation-rate probability distribution. Nevertheless, the highest probability remains associated with the true reference model (figure 3). The Kuhlback-Leibner information content varies along stratigraphic depth with high information content at intervals where the sedimentation rate is constant across the window size (3.3 m) and low where the sedimentation rate changes within the window. In any case, we note that the algorithm identifies the true (reference) sedimentation rates despite the high noise level, and that it reconstructs the large discontinuities between layers of constant rates quite well, with lower probability near abrupt sedimentation rate changes.

This study demonstrates that the `AstroComb` method extends the spectral misfit minimization strategy in a probabilistic framework, handling uncertainty propagation and parameter tuning with statistical rigor.

3.2 Real world data from the late Cambrian Alum Shale Formation

To illustrate the application of the multichannel, probabilistic Milankovitch period detector, `AstroComb`, we analysed high-resolution XRF data from a ∼21-meter long interval (67.2520 m - 88.0744 m) of the Fågeltofta-2 drill core through the Alum Shale Formation in southern Sweden obtained by Sørensen et al. (2020). Briefly, the XRF data was collected using an ITRAX core scanner from Cox Laboratories with 30 kV voltage and 50 mA current on a Rh tube. The XRF measurements were collected with a high scanning resolution of 0.2 mm

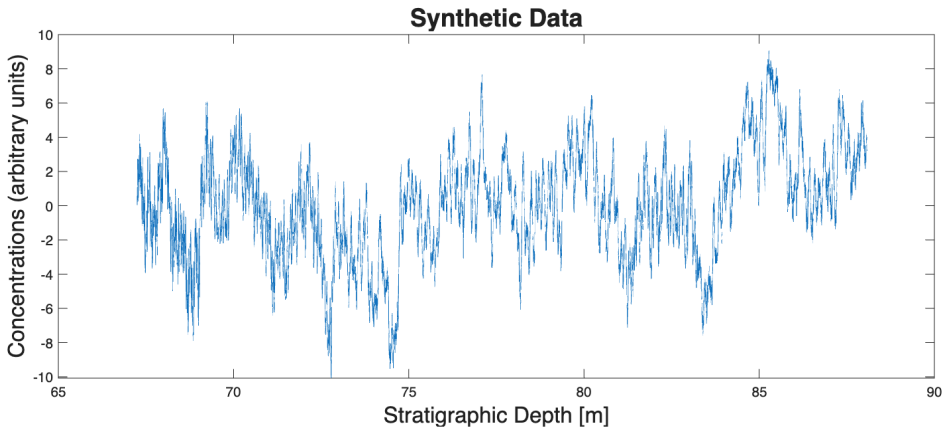

Figure 2: Synthetic data with 200% red noise used to test of the algorithm.

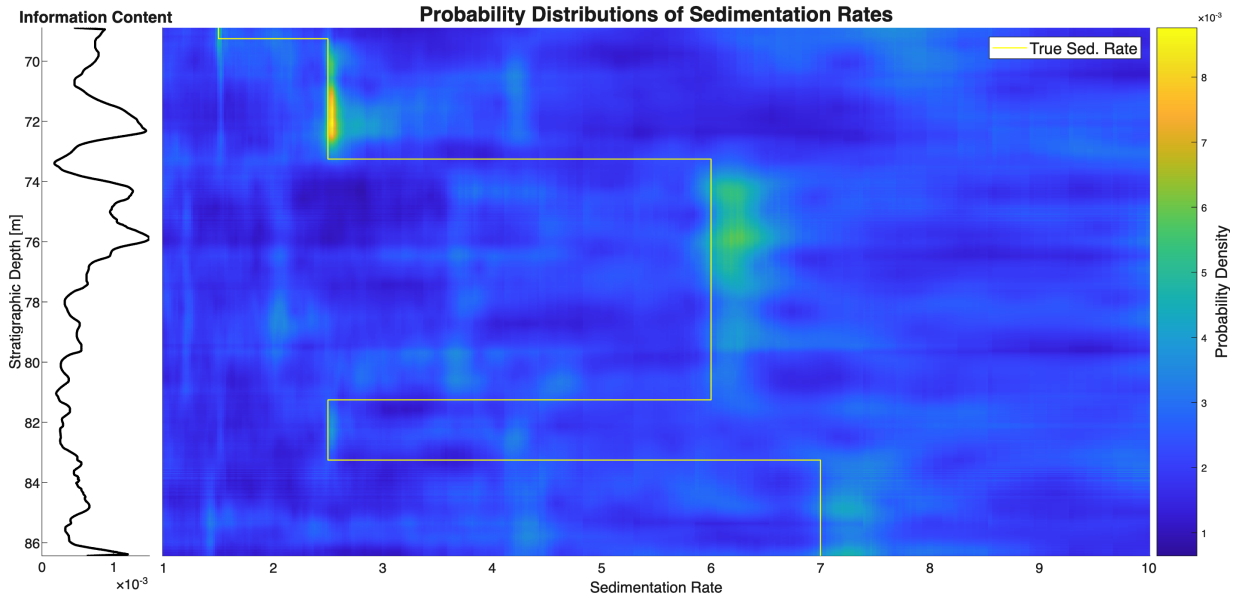

Figure 3: Probability density distributions of sedimentation rates computed from synthetic data with 200% red noise. The synthetic reference model is overlain to illustrate the fidelity of the reconstruction. Visually, the reconstructed sedimentation rates closely reproduce the true reference model. However, the results also demonstrate that noise, together with ambiguity in assigning a given cycle to different target periods, can introduce artifacts and lead to multimodal sedimentation-rate probability distributions for a given depth.

along the core and relatively long exposure time (7 sec/scan), producing signal reported as concentrations for 22 elements, incl. Al_2O_3, SiO_2, S, K_2O, CaO, TiO_2, V, MnO, Fe_2O_3, Ni, Cu, Zn, Ge, As, Rb, Sr, Y, Zr, Mo, Ba, Hf, and U. This extensive elemental dataset formed the basis for the spectral analysis. Figure 4 shows a subset (the top 40 mm) of the data from ∼19 m of core, yielding ∼90,000 measurements.

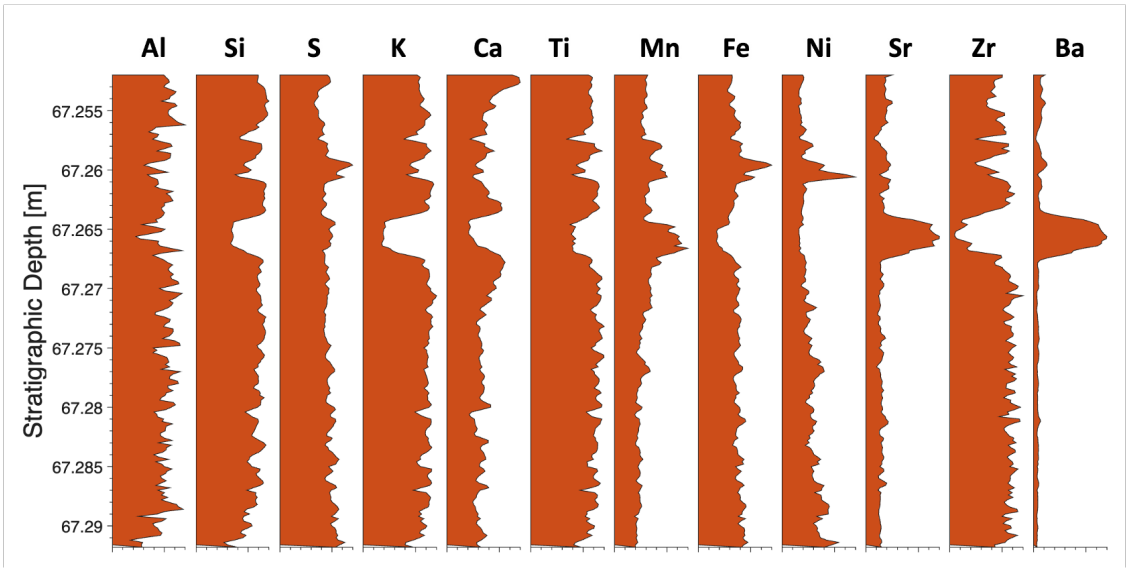

Figure 4: A selection of concentration profiles of the Fågeltofta-2 core, measured via XRF core scanning at 0.2 mm resolution. The records are all normalized to have the same maximum amplitude in the plot. The dataset spans approximately 19 meters of stratigraphy and comprises ∼ 90,000 individual measurements. Several profiles show well-developed quasi-periodic oscillations, which serve as the primary proxy for detecting orbitally forced sedimentary cycles in the subsequent astrochronological analysis.

3.2.1 Using one channel

We selected Al as the primary input because of its robustness as a proxy for detrital input and its strong spectral structure in preliminary analysis (Sørensen et al., 2020; Zhao et al., 2022). The depth series was detrended with a linear function. AstroComb was run using a window length of 3.3 m, stepped every 0.2 mm.

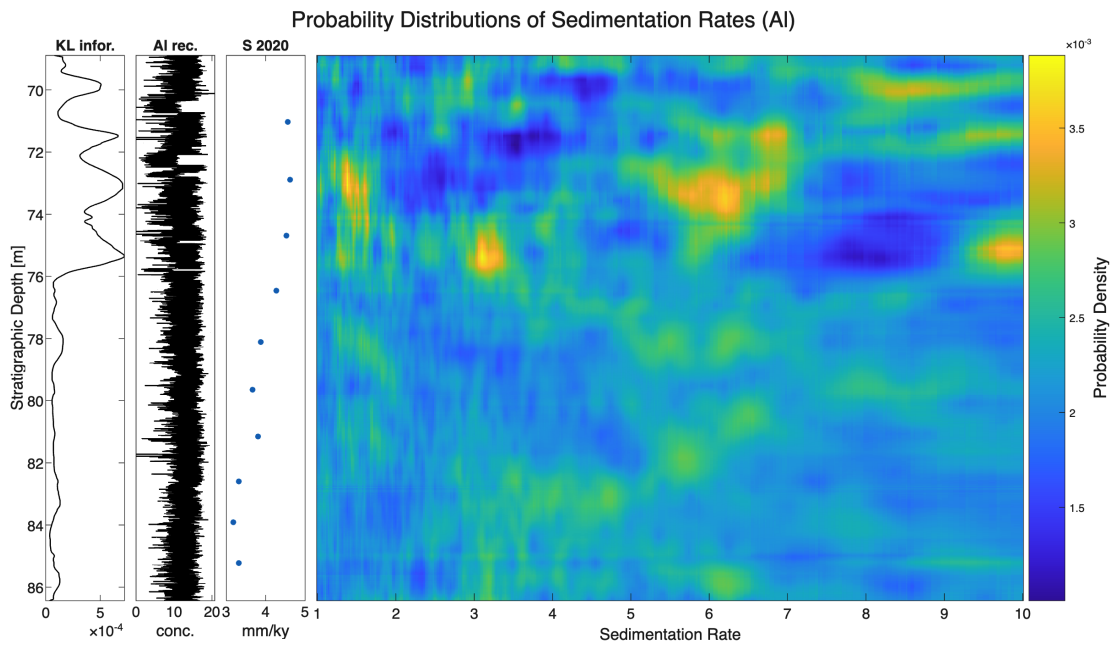

Figure 5: Sedimentation rate probability distribution for the Fågeltofta-2 core based on the Al record. The information content about Milankovitch cycles contained in the XRF data is quantified by the Kullback-Leibler measure.

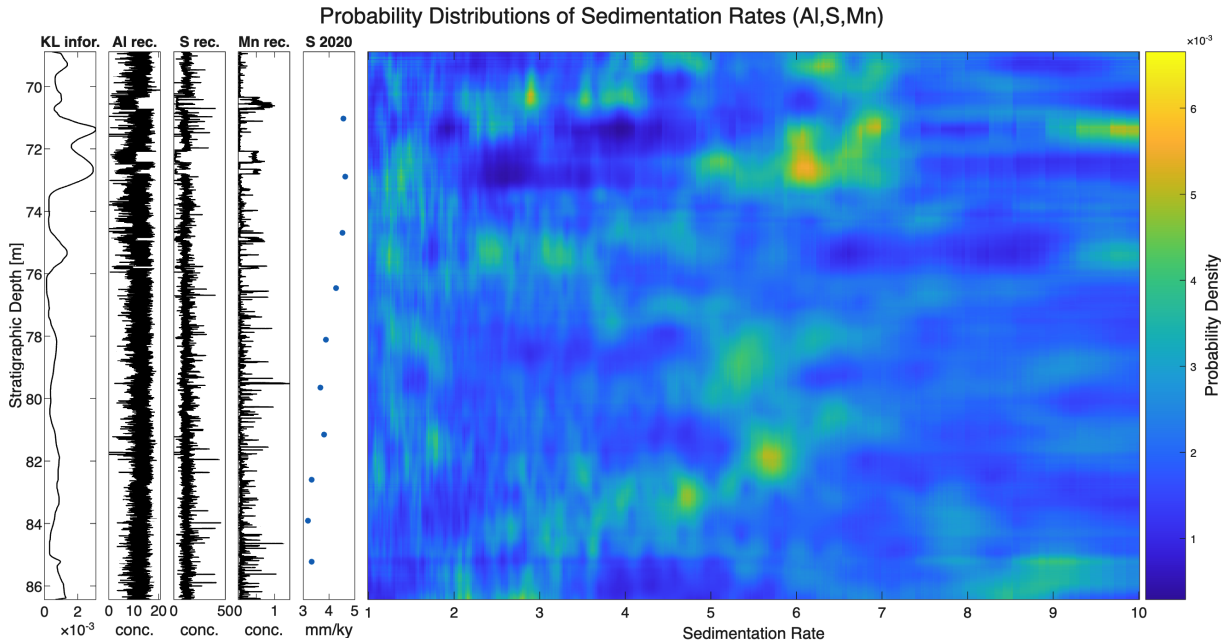

Figure 6: Probabilistic analysis of sedimentation rates in the Fågeltofta-2 core, based on simultaneous processing of S, Al, and Mn. Comparing to figure 5 it is clear that this multi-channel analysis has provided a higher resolution with more distinct peaks in the probability densities.

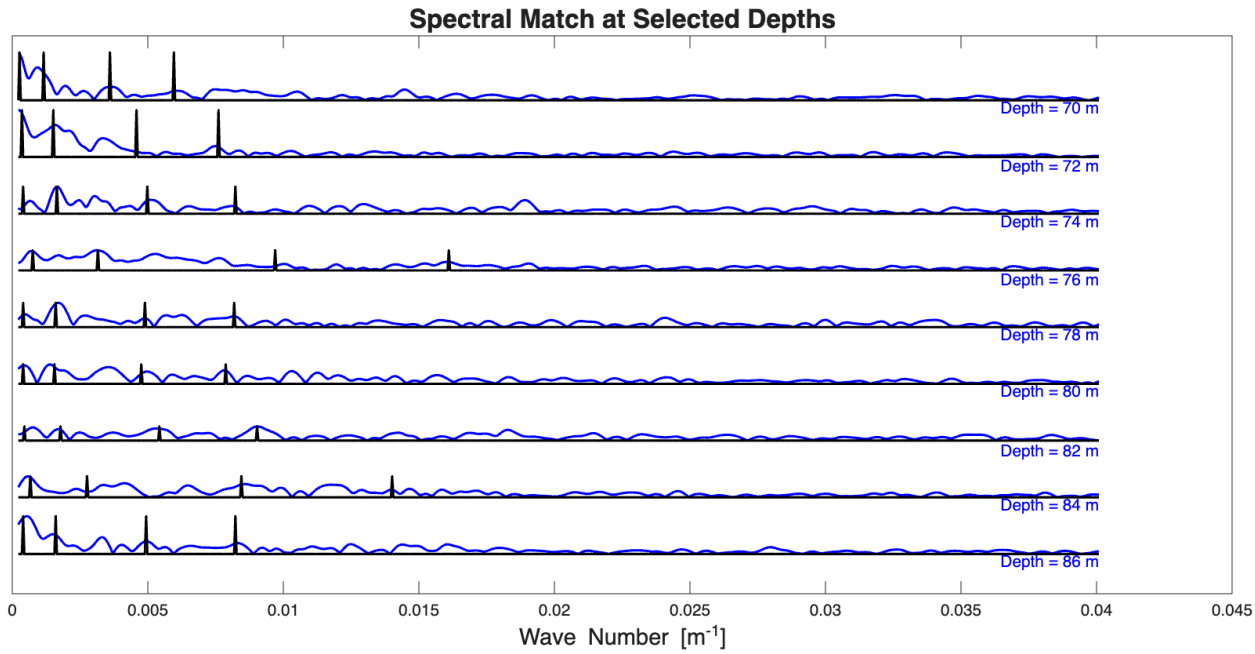

Figure 7: Spectral match at selected stratigraphic depths in the Fågeltofta-2 core. For every 2 m, the spectral lines corresponding to the best Milankovitch match are plotted (black) together with spectra of the Al content (blue) observed in windows centered at the depth.

The bulk sedimentation rate was *a priori* found within a range of realistic sedimentation rates from 1.0 to 10.0 mm/ky. As output, we show the a posteriori probability distribution of the sedimentation rates versus stratigraphic depth (figure 5), and selected spectral fits for each 2 m in the core (figure 7). The Kullback–Leibler information measure at each depth z indicates that the Al record above 76 m contains a stronger Milankovitch signal than the deeper intervals of the core. This corresponds to an approximately fourfold improvement in the fit between the data and the target spectrum above 76 m. Overall, figure 5 suggests that Milankovitch cyclicity is present throughout the core, as indicated by the non-zero information content, while sedimentation rates appear to vary across the section.

From the estimated sedimentation rates, a Milankovitch timescale and its uncertainty was derived (Figure 8), using the age of 496.595 Ma, consistent with Sørensen et al. (2020), at a stratigraphic depth of 86.005 m as a reference.

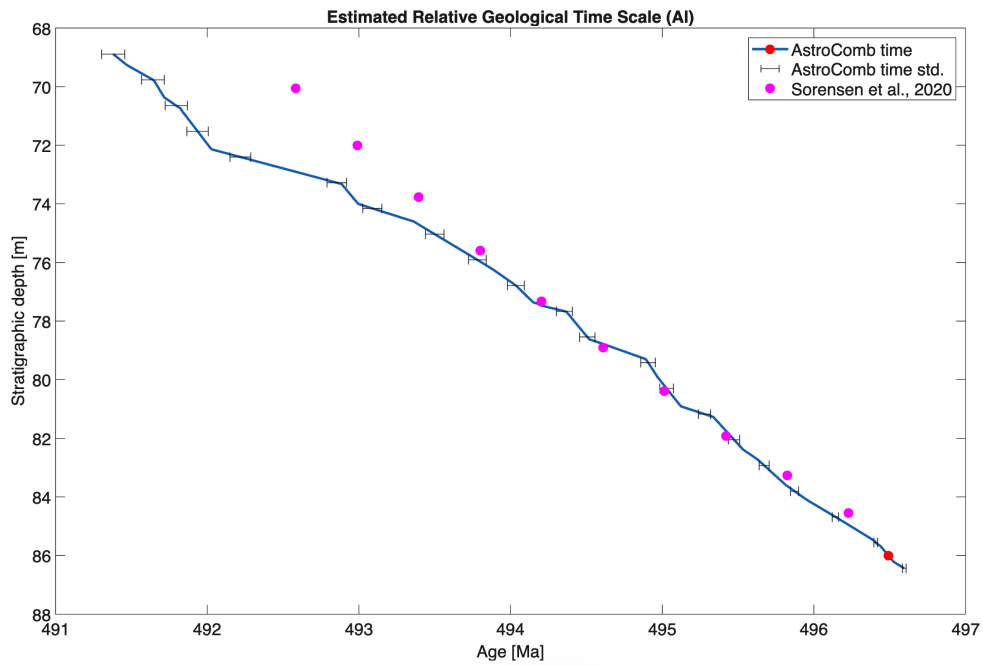

Figure 8: Estimated geological timescale and its uncertainty (standard deviations), based on probabilistic estimation of instantaneous sedimentation rates from the Al record in the Fågeltofta-2 core. The timescale is anchored at 86.005 m, corresponding to 496,595 ky (Sørensen et al., 2020). This anchor is marked with a red circle on the graph.

.

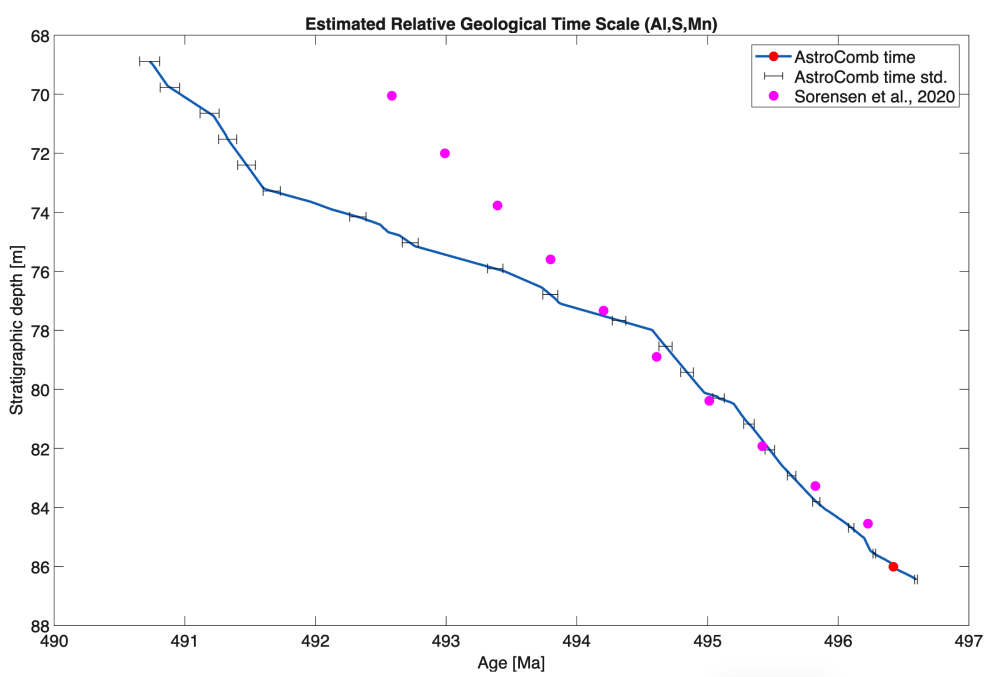

Figure 9: Relative timescale computed from the multi-channel data with records of S, Al and Mn.

This timescale enables the estimation of relative geological ages across the core, and allows depth-indexed chemical data to be analysed in the temporal domain, significantly enhancing our ability to interpret environmental transitions over geological timescales.

3.2.2 Using multiple channels

To demonstrate the capability of AstroComb for multichannel analysis, we applied the algorithm simultaneously to the S, Al, and Mn records. A central requirement in multichannel cyclostratigraphy is that the selected elemental channels provide independent information.

Often elements or element ratios are used as channels. Yet, XRF elements also covary because they share mineral hosts, are affected by dilution, or are linked through mathematical relationships, and such covariance can create a misleading impression of increased certainty rather than reflecting independent signals of Milankovitch forcing. For this reason, it is important to choose elements that are not cohosted, not simple dilutions of one another, and not strongly coupled, a choice that relies on expert knowledge of mineralogy and geochemistry. Al, S, and Mn meet these criteria in the Alum Shale. Although Al and S often show negative covariance, earlier studies demonstrate that each element records Milankovitch periodicities in intervals where the other does not (Sørensen et al., 2020; Zhao et al., 2022), indicating that their orbital signals are not only products of dilution or other non orbital processes.

The multichannel result, shown in figure 6, displays a clear improvement in spectral resolution compared to the single channel analysis in figure 5. High probabilities increase, low probabilities decrease, and several secondary peaks that previously suggested alternative solutions are reduced or absent. The information content follows the same general pattern as before but increases by roughly an order of magnitude when three channels are used instead of one. The corresponding relative time scale in figure 9 is similar to that in figure 8, but with greater detail and a slightly longer total duration.

These results support the use of high resolution XRF data combined with probabilistic spectral inversion as a powerful approach for extracting geochronological information from ancient sedimentary archives.

4 Discussion

4.1 Limitations

Nonetheless, some limitations must be acknowledged. The assumed orbital target periods are model-based. While the tuning strategy often relies on the 405 ky eccentricity cycle as a stable chronometer, potential shifts in Earth's rotational parameters due to e.g. tidal dissipation effects could introduce biases.

Our algorithm is based on the assumption that prior information about the spectral peak identification process can be provided, and that it adequately describes the way Milankovitch periods are identified by human analysts. According to our synthetic tests, and the good consistency of our Fågeltofta-2 results with results from previous studies, it works well, but it is advisable to carefully check results obtained in new cases, particularly to what extent they are compatible with other, independent knowledge about the geological scenario considered.

There are also some fundamental assumptions behind Milankovitch analysis that apply to any method. Milankovitch cycles are (quasi-)periodic, but not sinusoidal. This means that a hypothetical, noise-free Milankovitch spectrum will, in general, contain spectral components outside the main Milankovitch frequencies (Sinnesael et al., 2018). These components are generally disregarded in Milankovitch analysis programs, including `AstroComb`. More seriously, the Earth's sedimentary system is highly nonlinear and is therefore expected to produce additional periods that are sums and differences of the main Milankovitch cycles. The amplitudes of such periods could be significant, but they are ignored by our algorithm, since we are not interested in the amplitudes, only in the wave numbers. An additional problem with the non-linearity of the sedimentary system is that, even if we know the amplitudes of the input Milankovitch signal, the output amplitudes observed in boreholes are entirely unknown. This was the background for the way that we designed our spectral fit algorithm, (e.g. somewhat agnostic to the amplitude of the recorded periodicities) .

Last, but not least, it is important to remember that Milankovitch cycle identification is a *difficult* problem. The signal-to-noise ratio is generally very low, and the problem is often similar to finding a needle in a hay stack. Such problems are prone to detrimental human biases, but `AstroComb` is designed with the aim of quantifying the analysis, and casting the problem as a probabilistic inference problem, so as to avoid such biases. It generally provides several plausible solutions for the sedimentation rates at given depths, allowing the user to choose, based on geological/stratigraphic knowledge.

4.2 Broader Implications

The `AstroComb` algorithm has discovered abrupt changes in sedimentation rate in the Fågeltofta-2 core making predictions to guide sedimentologist in reconstructing pulses of sedimentation from geological archives. Sedimentation rate shifts in the Alum shale Formation (incl. Billegrav-2 and Fågeltofta) are correlated to relative sea level changes obtained from sequence stratigraphy (Sørensen et al., 2020). Yet, previous sedimentation rate estimates obtained using eCoco and a smoothing spline fit on visually profound periods in the wavelet spectrum unavoidably induced some degree of smoothing of the sedimentation rate, which may give a false impression of the actual sedimentation rate changes. With AstroComb, sedimentation rate changes are not necessarily changing smoothly across stratigraphy.

As sedimentation rate is a fundamental parameter characterizing a sedimentary environment and a factor that serves as a first order control on organic matter preservation, `AstroComb` may help engaging sedimentologists with a new relative chronometer. Also, we envision to use it in combination with geochemical information about sedimentation rate changes.

5 Conclusion

The algorithm contributes methodologically to the field of deep-time astrochronology by offering a multi-channel, probabilistic method for estimation of astronomically constrained timescales. At the same time we offer critical quality control of the data, allowing the user to evaluate how much Milankovich information can actually be detected in the XRF-derived

elemental records. The framework established here provides a robust platform for exploring the causes and consequences of climatic, geochemical, and evolutionary change in Earth's early history.

6 Code and Data Availability

The exact version of the program used to generate all results in this paper, together with the input data, the scripts used to run the model, and the scripts used to produce the plots for all simulations, is available at https://doi.org/10.5281/zenodo.17966227 under the licence GNU General Public License v3.0.

7 Author Contributions

Iris Fernandes and Klaus Mosegaard led the conceptualization of the study and the development of the methodology, including algorithm design, numerical analysis, inverse problem formulation, and the integration of uncertainty quantification. They implemented the data processing and analysis pipeline, contributed to the overall methodological design, and drafted the original manuscript. Tais W. Dahl and Aske Sørensen contributed to the theoretical framework and provided critical input on the geochemical and geological interpretation and analysis. Mohammad Youssof contributed to algorithm parameterization and optimization. Nicholas Thibault contributed with geochronological insights in the analysis. Klaus Mosegaard and Tais W. Dahl obtained funding for the project.

8 Acknowledgments

The authors thank Marie-Louise Siggaard Andersen at the core scanning XRF laboratory at Globe for discussions on data quality, and Mattis Ring Westergaard for insightful comments and corrections to the code. Agnete K. H. Abildtrup and Astrid Juel Bojsen-Møller assisted at the core scanner when evaluating data uncertainty. We acknowledge funding from the Villum Data Synergy Programme (project no. 50114).

References

Farhat, M., Auclair-Desrotour, P., Boué, G., and Laskar, J. (2022). The resonant tidal evolution of the earth–moon distance. *Astronomy Astrophysics*, 665:L1.

Hays, J. D., Imbrie, J., and Shackleton, N. J. (1976). Variations in the earth's orbit: Pacemaker of the ice ages. *Science*, 194(4270):1121–1132.

Herbert, T. D. (1994). Reading orbital signals distorted by sedimentation: models and examples. In de Boer, P. L. and Smith, D. G., editors, *Orbital Forcing and Cyclic Sequences*, volume 19 of *Special Publication*, pages 483–507. International Association of Sedimentologists.

Hinnov, L. A. (2013). Cyclostratigraphy and its revolutionizing applications in the earth and planetary sciences. *Geological Society of America Bulletin*, 125(11–12):1703–1734.

Hoang, N., Laskar, J., Hara, N. C., Wu, Y., Sultanov, A., Sinnesael, M., Westerhold, T., and Bujons, P. (2025). Astrogeofit: A genetic algorithm and bayesian approach for the astronomical calibration of the geological timescale. *Paleoceanography and Paleoclimatology*, 40(8):e2024PA005021.

Kemp, D. B. and Sexton, P. F. (2014). Time-scale uncertainty of abrupt events in the geologic record arising from unsteady sedimentation. *Geology*, 42(10):891–894.

Kullback, S. and Leibler, R. A. (1951). On information and sufficiency. *The Annals of Mathematical Statistics*, 22:79–86.

Laskar, J. (2020). Chapter 4 - astrochronology. In Gradstein, Felix M. Gradstein, J. G. O. M. D. S. G. M. O., editor, *Geologic Time Scale 2020*, page 139–158. Elsevier, Amsterdam.

Laskar, J., Fienga, A., Gastineau, M., and Manche, H. (2011). A new orbital solution for the long-term motion of the earth. *Astronomy Astrophysics*, 532:A89.

Laskar, J., Robutel, P., Joutel, F., Gastineau, M., Corrêia, A. C. M., and Levrard, B. (2004). A long-term numerical solution for the insolation quantities of the earth. *Astronomy Astrophysics*, 428(1):261–285.

Li, M., Kump, L. R., Hinnov, L. A., and Mann, M. E. (2018). Tracking variable sedimentation rates and astronomical forcing in phanerozoic paleoclimate proxy series with evolutionary correlation coefficients and hypothesis testing. *Earth and Planetary Science Letters*, 501:165–179.

Ma, C., Meyers, S. R., and Sageman, B. B. (2017). Theory of chaotic orbital variations confirmed by cretaceous geological evidence. *Nature*, 542:468–470.

Malinverno, A., Erba, E., and Herbert, T. D. (2010). Orbital tuning as an inverse problem: Chronology of the early aptian oceanic anoxic event 1a (Selli Level) in the Cismon APTICORE. *Paleoceanography*, 25(2):PA2203.

Malinverno, A. and Meyers, S. R. (2024). Bayesian estimation of past astronomical frequencies, lunar distance, and length of day from sediment cycles. *Geochemistry, Geophysics, Geosystems*, 25:e2023GC011176.

Meyers, S. R. (2015). The evaluation of eccentricity-related amplitude modulation and bundling in paleoclimate data: An inverse approach for astrochronologic testing and timescale optimization. *Paleoceanography*, 30(12):1625–1640.

Meyers, S. R. and Malinverno, A. (2018). Proterozoic milankovitch cycles and the history of the solar system. *Proceedings of the National Academy of Sciences*, 115(25):1717689115.

Meyers, S. R., Sageman, B., and Hinnov, L. (2001). Integrated quantitative stratigraphy of the cenomanian-turonian bridge creek limestone member using evolutive harmonic analysis and stratigraphic modeling. *Journal of Sedimentary Research*, 71:627–643.

Meyers, S. R. and Sageman, B. B. (2007). Quantification of deep-time orbital forcing by average spectral misfit. *American Journal of Science*, 307(5):773–792.

Munnecke, A., Westphal, H., Elrick, M., and Reijmer, J. J. G. (2001). The mineralogical composition of precursor sediments of calcareous rhythmites: A new approach. *International Journal of Earth Sciences*, 90(4):795–812.

Pälike, H., Norris, R. D., Herrle, J. O., Wilson, P. A., Coxall, H. K., Lear, C. H., Shackleton, N. J., Tripati, A. K., and Wade, B. S. (2006). The heartbeat of the oligocene climate system. *Science*, 314:1894–1898.

Paola, C. (2016). A mind of their own: Recent advances in autogenic dynamics in rivers and deltas. *SEPM Special Publications*, 106:5–17.

Peng, C., Zou, C., Wu, H., Zhang, S., Kouamelan, K. S., and Wang, C. (2023). Evaluating geophysical logs as proxies for cyclostratigraphy in lacustrine deposits using power ratio accumulation. *Palaeogeography, Palaeoclimatology, Palaeoecology*, 614:111428.

Ripepe, M. and Fischer, A. G. (1991). Stratigraphic rhythms synthesized from orbital variations. In Franseen, E. K., Watney, W. L., Kendall, C. G. S. C., and Ross, W., editors, *Sedimentary Modeling*. Kansas Geological Survey.

Schiffelbein, P. and Dorman, L. (1986). Spectral effects of time–depth nonlinearities in deep sea sediment records: a demodulation technique for realigning time and depth scales. *Journal of Geophysical Research*, 91:3821–3835.

Sinnesael, M., Zivanovic, M., De Vleeschouwer, D., and Claeys, P. (2018). Spectral moments in cyclostratigraphy: Advantages and disadvantages compared to more classic approaches. *Paleoceanography and Paleoclimatology*, 33(5):493–510.

Sinnesael, M., Zivanovic, M., De Vleeschouwer, D., Claeys, P., and Schoukens, J. (2016). Astronomical component estimation (ace v.1) by time-variant sinusoidal modeling. *Geoscientific Model Development*, 9(10):3517–3531.

Sørensen, A. L., Nielsen, A. T., Thibault, N., Zhao, Z., Schovsbo, N. H., and Dahl, T. W. (2020). Astronomically forced climate change in the late cambrian. *Earth and Planetary Science Letters*, 548:116475.

Trayler, R. B., Meyers, S. R., Sageman, B. B., and Schmitz, M. D. (2024). Bayesian integration of astrochronology and radioisotope geochronology. *Geochronology*, 6:107–123.

Waltham, D. (2015). Milankovitch period uncertainties and their impact on cyclostratigraphy. *Journal of Sedimentary Research*, 85:990–998.

Zhao, Z., Pang, X., Zou, C., Dickson, A. J., Basu, A., Guo, Z., Pan, S., Nielsen, A. T., Schovsbo, N. H., Jing, Z., and Dahl, T. W. (2023). Dynamic oceanic redox conditions across the late cambrian spice event constrained by molybdenum and uranium isotopes. *Earth and Planetary Science Letters*, 604:118013.

Zhao, Z., Thibault, N. R., Dahl, T. W., Schovsbo, N. H., Sørensen, A. L., Rasmussen, C. M. , and Nielsen, A. T. (2022). Synchronizing rock clocks in the late cambrian. *Nature Communications*, 13:1990.

Zhou, Z., Meyers, S. R., Maloof, A. C., Li, M., et al. (2024). Earth–moon dynamics from cyclostratigraphy reveals possible ocean tide resonance in the mesoproterozoic era. *Science Advances*, 10(50):e adn7674.